Theory of shock wave propagation during laser ablation

Zhaoyan Zhang and George Gogos
Department of Mechanical Engineering, University of Nebraska-Lincoln, Lincoln, Nebraska 68588, USA
(Received 4 February 2004; published 8 June 2004)

Laser ablation consists of three coupled processes: (i) heat conduction within the solid, (ii) flow through a discontinuity layer (evaporation wave) attached to the solid surface, and (iii) shock wave expansion of the laser induced plume. In this paper, a one-dimensional solution for all three coupled processes is presented. The heat conduction and the evaporation wave are solved numerically. The shock wave expansion of the laser induced plume, however, is solved analytically, to our knowledge, for the first time; analytical solutions for the classic Riemann problem have been employed to solve the transient propagation of the strong shock wave. This model provides a sound theoretical basis for the analysis of the laser ablation process. The temperature, pressure, density, and velocity of the laser induced plume at different laser intensities, back temperatures, back pressures, and ambient gas species are calculated. The effects of the laser intensity, back temperature, back pressure, and ambient gas species are analyzed. The theoretical results provide insight into experimental results available in the literature.

DOI: 10.1103/PhysRevB.69.235403 PACS number(s): 47.40.−x

INTRODUCTION

Laser ablation describes the explosive laser-material interaction. The process has many applications in science and engineering, such as pulsed laser deposition and micromachining. When the laser-pulse duration is in the microsecond or longer range and the laser intensity is less than $\approx 10^6$ W/cm^2, material is removed through evaporation with negligible ionization. The evaporation process of a solid was first studied by Ready[1] and Anisimov[2] in the 1960s. It has been shown that the surface temperature increases logarithmically with increasing laser intensity, while the rate of ablation increases linearly with the laser intensity, barring heat losses.[3] Within the Knudsen layer, the ablated material undergoes a rapid phase change from solid to vapor and the vapor expands into an evaporation wave. This process has been studied by Anisimov[2] and Knight.[4] When the laser-pulse duration is in the nanosecond or shorter range and the laser intensity exceeds $\approx 10^9$ W/cm^2, a considerable fraction of the evaporated atoms may be ionized, as the high-temperature and high-pressure vapor expands into a shock wave. The dense plasma formed in front of the solid target absorbs a substantial fraction of the laser light and may completely shield the solid target at extremely high laser intensities. In the pioneering work of Krokhin,[5] the physical mechanism of evaporation coupled with vapor/plasma expansion was formulated.

More recently, a large number of studies appeared in the literature that examined various aspects of the laser ablation process. The relatively few analytical studies that have been carried out did not model the expansion process of the laser induced plume. Tokarev *et al.*[6] proposed an analytical thermal model of ultraviolet laser ablation. Their model took into account the factors, such as moving interface and Arrhenius dependence of ablation rate, that previous analytical studies had not treated simultaneously. Dahmani[7,8] developed scaling laws for mass ablation rate, recoil pressure with laser intensity, laser wavelength, and target atomic number.

Numerical simulations of laser-material interaction have been conducted by many researchers as well. Kar and Mazumder[9] developed a model that simulates the nanoscale particles generated in the laser induced plume using a droplet-growth theory. Ho, Grigoropoulos, and Humphrey[10,11] studied the heat transfer, fluid flow phenomena, and subsequent ionization in pulsed laser processing of metals. Zhang, Han, and Dulikravich proposed a two-dimensional numerical model of the laser ablation process. A flux vector splitting scheme is used to capture the shock wave expanion process of the laser induced plume. Mao *et al.*[13] developed a numerical model to simulate the picosecond laser induced plume. In a numerical model of the laser induced plume, developed by Bulgakov and Bulgakova,[14] plasma dynamics are described in the framework of two-temperature approximation.

During the 1990s, a number of studies were focused on the structure of the laser induced plume. Kelly and Braren[15] first proposed the contact surface and expansion front associated with laser ablation. Kelly *et al.*[16] and Dyer *et al.*[17] showed the two-layered structure of the laser induced plume using a probe laser photograph. Jeong, Greif, and Russo[18] showed the existence of a contact surface by obtaining the structure of the laser induced plume numerically.

A number of experimental studies have examined the effects of the ambient conditions on laser ablation and are particularly relevant to the present study. It is well known that the ambient gas reduces the energy of the vapor flux and provides a high flux of background gas. Geohegan[19] noted that raising the background pressure sharpens the plume boundary and slows the plume propagation. Mao, Chan, and Russo[20] investigated the effects of the background pressure and ambient gas composition on laser ablation. It was shown that the ionization of the laser induced plume increases with a decrease in the background pressure. The laser induced plume has a lower degree of ionization for helium background gas than for argon. Mendes and Vilar[21] studied the influence of background gas on the laser ablation of ceramics both experimentally and numerically. They found that the ablation rate decreases with increasing molecular weight and pressure of the ambient gas. Harilal[22] observed that the am-

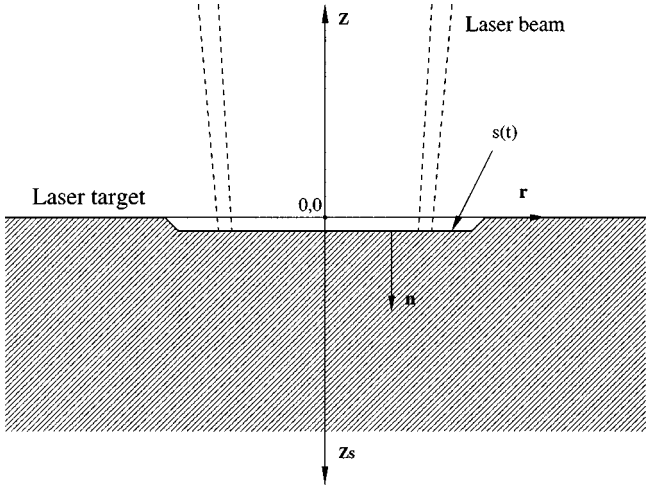

FIG. 1. Schematic and coordinate system of the laser ablation process.

bient pressure and laser intensity have opposite effects on the expansion dynamics of the laser ablated plume. Braun, Zimmer, and Bigl[23] found that the ablation rate decreases with increasing ambient temperature, however, no physical explanation was provided.

A theoretical model can provide a sound basis for the analysis of the structure of the laser induced plume and of the effects of the ambient conditions on laser ablation. In the present paper, a one-dimensional model of the laser induced evaporation is presented. The heat conduction and the evaporation wave are solved numerically. The shock wave expansion of the laser induced plume, however, is solved analytically, to our knowledge, for the first time. The solution for the classic Riemann problem is employed to solve the transient shock wave propagation during laser ablation. This model properly captures the contact surface in the laser induced plume and provides insight into other experimental results available in the literature. The temperature, pressure, density, and velocity of the laser induced plume are calculated for typical laser parameters and ambient conditions for pulsed laser deposition. The effects of the laser intensity, back temperature, back pressure, and ambient gas species are analyzed.

PROBLEM FORMULATION AND SOLUTION APPROACH

A schematic of the problem under consideration is given in Fig. 1. The formulation of the physical mechanism of evaporation coupled with vapor expansion follows that of Krokhin.[5] A transient one-dimensional model can be used to describe the heat diffusion process within the solid:

$$\frac{\partial T}{\partial t} - v_0 \frac{\partial T}{\partial z_s} = \frac{1}{\rho_0 c_p}\left[\frac{\partial}{\partial z_s}\left(k\frac{\partial T}{\partial z_s}\right) - \left(\frac{\partial Q_l}{\partial z_s}\right)\right], \tag{1}$$

where t is time, z_s is the coordinate in the direction of the laser beam, T is temperature, v_0 is the ablation velocity in the z_s direction, $\alpha_s = k/\rho_0 c_p$ is the thermal diffusivity of the solid material, $Q_l = (1-R)Qe^{-\kappa[Z_s - s(t)]}$ is the laser intensity penetrating into the solid, $s(t)$ is the thickness of the ablated solid, Q is the laser intensity at the surface of the solid, R is the reflectance of the solid, and κ is the absorption coefficient of the solid.

The initial and boundary conditions are

$$t = 0, \quad T = T_\infty, \tag{2}$$

$$z_s = s(t), \quad k\mathbf{n}\cdot\nabla T = \rho_0 L v_0, \tag{3}$$

$$z_s \to \infty, \quad T \to T_\infty, \tag{4}$$

where L is the latent heat of the material, ρ_0 is its density, and T_∞ is the ambient temperature.

The ablation velocity v_0 is related to the surface temperature by an Arrhenius equation[3]

$$v_0 = \frac{p_b \exp\left[\frac{L}{R}\left(1/T_b - 1/T_s\right)\right]}{\rho_0\sqrt{2\pi k_B T_s/m}} \tag{5}$$

$$= \frac{p_0}{\rho_0\sqrt{2\pi k_B T_s/m}}, \tag{6}$$

where m is the mass of an evaporated molecule, k_B is Boltzmann's constant, T_s is the surface temperature, R is the gas constant, p_b is the saturation pressure at the equilibrium boiling temperature T_b, and p_0 is the vapor pressure at the surface temperature.

The evaporation wave attached to the solid surface obeys the laws of conservation of mass, momentum, and energy, which can be expressed as[5]

$$-\rho_0 v_0 = \rho(v - v_0), \tag{7}$$

$$p_0 = p - \rho_0 v_0 v, \tag{8}$$

$$-\rho_0 v_0 e_0 = -\rho_0 v_0 (e + v^2/2) + pv, \tag{9}$$

where ρ is the density, e is the mass-specific internal energy, and p is the pressure. The subscript 0 indicates values for the condensed phase, whereas values for the gaseous phase are indicated without subscript. The values for the condensed phase are calculated by solving Eqs. (1)–(6). The gaseous phase is assumed to obey the ideal gas law. Therefore, its pressure can be expressed by $p = \rho RT$.

For lasers operating at ultraviolet wavelength, the absorption of the laser light by the laser induced plume of moderately high temperature is negligible. The expansion process of the laser induced plume can be expressed by the following equations:

$$\frac{\partial \rho}{\partial t} + \nabla\cdot(\rho\mathbf{u}) = 0, \tag{10}$$

$$\rho\frac{\partial \mathbf{u}}{\partial t} + \rho(\mathbf{u}\cdot\nabla)\mathbf{u} + \nabla p = 0, \tag{11}$$

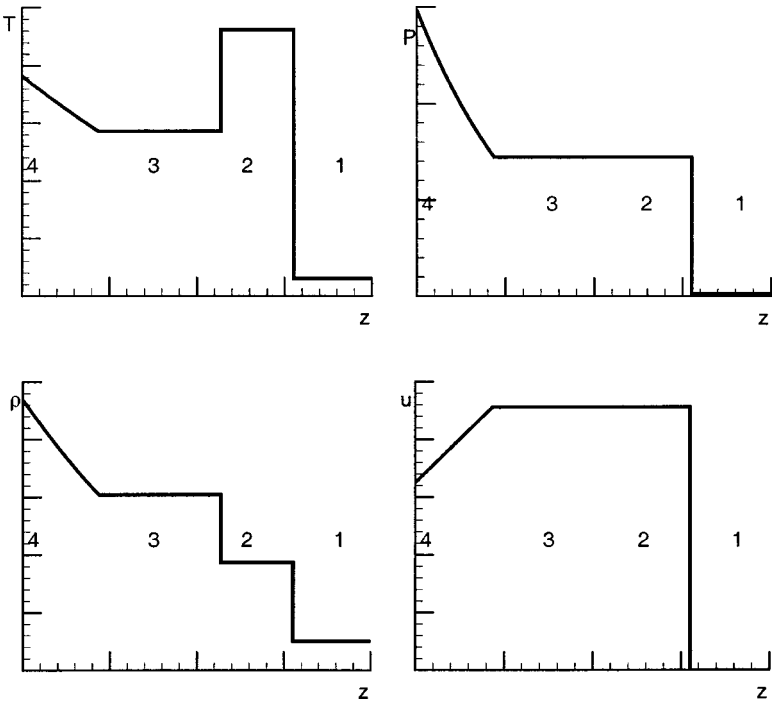

FIG. 2. Typical profiles of thermodynamic and flow properties of the laser induced plume.

$$\rho\frac{\partial \epsilon}{\partial t} + \rho\mathbf{u}\cdot\nabla\epsilon + p\nabla\cdot\mathbf{u} = 0. \tag{12}$$

Here, $\mathbf{u}$ is the fluid velocity and ϵ is the mass-specific total energy of the vapor.

It should be noted that the interactions of laser light of longer wavelength and the laser induced plume of extremely high temperature may be significant. These extremely complicated interactions add a source term in the conservation of energy equation and can only be simulated by numerical models.

The one-dimensional conduction equation can be solved using an integral method. After the temperature field of the solid is found, the conservation equations of mass, momentum, and energy of the discontinuity layer can be solved using a simple iterative procedure to provide the boundary conditions for the expansion process. The solution approach for the conduction equation and for the conservation equations of the discontinuity layer has been discussed in detail elsewhere,[12,24] and the readers are referred to the original references. The expansion of the high-temperature vapor is a predominantly one-dimensional process[12] and is similar to the classic Riemann problem. The high-temperature and high-pressure vapor generated by the laser heating expands rapidly into the ambient gas and creates a strong shock wave. In the meantime, a rarefaction wave generated from the quiescent gas propagates in the opposite direction at the local speed of sound into the high-temperature vapor. The shock wave and the rarefaction wave interact to establish a common pressure and velocity for the gas downstream of these waves. The profiles of thermodynamic and flow properties of the laser induced plume are shown qualitatively in Fig. 2. The horizontal axis indicates distance from the ablated surface. The difference between the laser induced plume expansion and the classic Riemann problem is that the flow velocity is finite at the discontinuity layer for the laser induced plume, whereas the flow velocity is zero for the classic Riemann problem. In order to use the Riemann problem solutions, the conditions at the stagnation point should be extrapolated. The equations governing the rarefaction wave and the shock wave can be found in a number of standard compressible fluid mechanics textbooks, e.g., Ref. 25. The temperature, pressure, density, and velocity profiles of the laser induced plume can be determined as described below.

(1) The thermodynamic properties at the stagnation point can be extrapolated from those which are immediately adjacent to the discontinuity layer. The rarefaction wave is isentropic and follows the relation

$$\frac{a}{a_4} = 1 - \frac{\gamma_4 - 1}{2}\left(\frac{u}{a_4}\right), \tag{13}$$

where a is the speed of sound immediately adjacent to the discontinuity layer and γ is the ratio of specific heats. The subscript 4 indicates values for the stagnation point. After the speed of sound at the stagnation point is determined, the pressure, temperature, and density at the stagnation point can be readily calculated.

(2) Once the thermodynamic properties at the stagnation point are determined, the shock wave strength p_2/p_1 should be calculated. The subscripts 1 and 2 indicate values at the ambient gas and the shock wave front (regions 1 and 2 in Fig. 2, respectively). The shock wave strength is related to the ratio of the stagnation pressure and the ambient pressure by

TABLE I. Material properties of graphite.

T_b(K)	α_s(m^2/s)	ρ_o(kg/m^3)	L(J/kg)
4000	5×10^{-6}	1.73×10^3	34.5×10^6
c_p(J/kgK)	$\kappa(\mu\text{m}^{-1})$	γ	R
2090	10	1.67	0.9

$$\frac{p_4}{p_1}=\frac{p_2}{p_1}\left\{1-\frac{(\gamma_4-1)(a_1/a_4)(p_2/p_1-1)}{\sqrt{2\gamma_1[2\gamma_1+(\gamma_1+1)(p_2/p_1-1)]}}\right\}^{2\gamma_4/(\gamma_4-1)}, \tag{14}$$

where p is the pressure. All the other shock wave properties are related to the shock wave strength and can be calculated using the following equations:

$$\frac{T_2}{T_1}=\frac{p_2}{p_1}\left(\frac{\frac{\gamma_1+1}{\gamma_1-1}+\frac{p_2}{p_1}}{1+\frac{\gamma_1+1}{\gamma_1-1}\frac{p_2}{p_1}}\right), \tag{15}$$

$$\frac{\rho_2}{\rho_1}=\frac{1+\frac{\gamma_1+1}{\gamma_1-1}\frac{p_2}{p_1}}{\frac{\gamma_1+1}{\gamma_1-1}+\frac{p_2}{p_1}}, \tag{16}$$

$$M_s=\sqrt{\frac{\gamma_1+1}{2\gamma_1}\left(\frac{p_2}{p_1}-1\right)+1}, \tag{17}$$

$$u_p=\frac{a_1}{\gamma_1}\left(\frac{p_2}{p_1}-1\right)\left(\frac{\frac{2\gamma_1}{\gamma_1+1}}{\frac{p_2}{p_1}+\frac{\gamma_1-1}{\gamma_1+1}}\right)^{1/2} \tag{18}$$

Here, M_s is the shock wave Mach number and u_p is the velocity of the mass motion behind the shock wave, which is induced by the shock wave propagating into a stagnant gas.

(3) The strength of the rarefaction wave is defined as p_3/p_4. It is related to the shock wave strength and the ratio of the stagnation pressure and the ambient pressure by

$$\frac{p_3}{p_4}=\frac{p_3/p_1}{p_4/p_1}=\frac{p_2/p_1}{p_4/p_1}. \tag{19}$$

Subscript 3 indicates values at the wake of the rarefaction wave (region 3 in Fig. 2). Since the rarefaction wave is isentropic, other thermodynamic properties immediately behind the rarefaction wave can be found from the isentropic relations

$$\frac{p_3}{p_4}=\left(\frac{\rho_3}{\rho_4}\right)^{\gamma_4}=\left(\frac{T_3}{T_4}\right)^{\gamma_4/(\gamma_4-1)}. \tag{20}$$

(4) The rarefaction wave is moving toward the left, while the mass motion is moving toward the right. Physically, the propagation of a local part of the rarefaction wave is the local speed of sound superimposed on top of the local mass motion; that is, all portions of the rarefaction wave are propagating at a velocity of $u-a$ relative to the laboratory. This can be expressed by

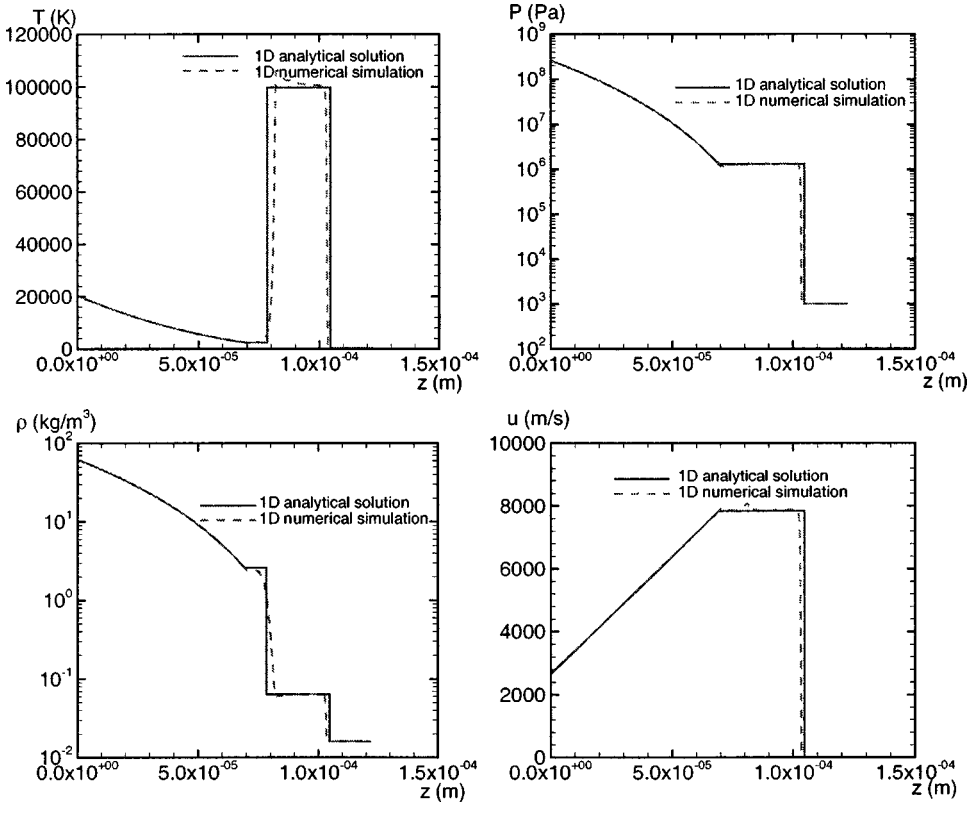

FIG. 3. Comparisons between analytical and numerical predictions of temperature, pressure, density, and velocity of a laser induced plume.

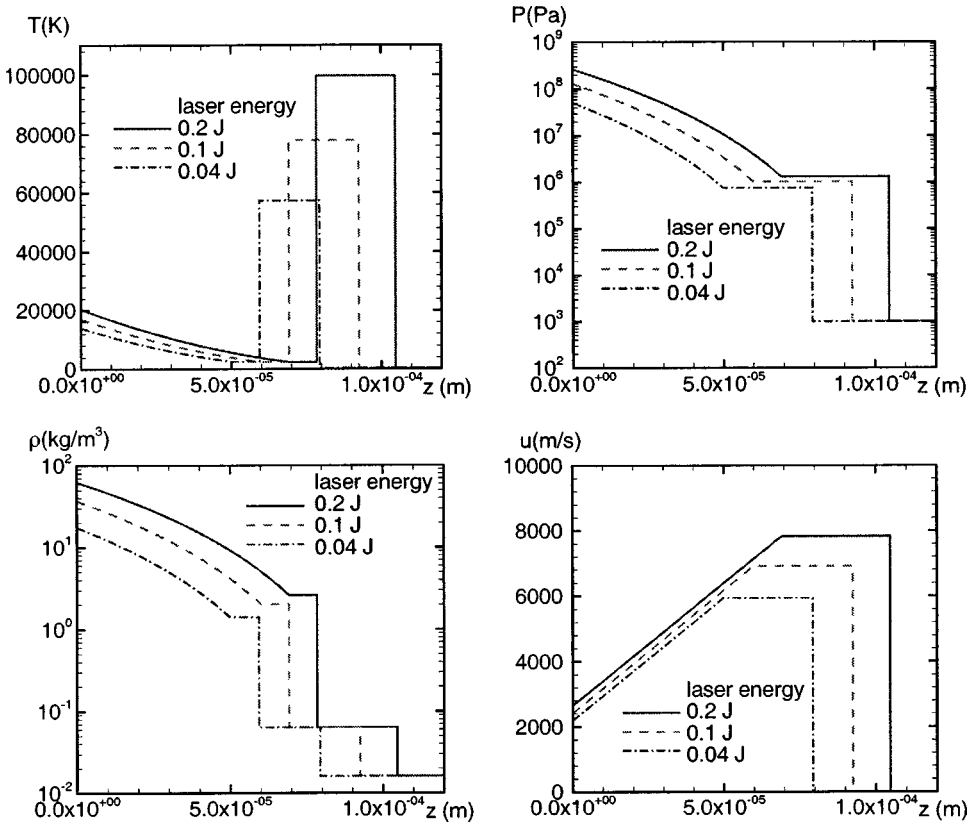

FIG. 4. Profiles of temperature, pressure, density, and velocity of the laser induced plume for different laser energies.

$$z = (u - a)t = \left(u - a_4 + \frac{\gamma_4 - 1}{2}u\right)t. \tag{21}$$

The above equation shows that u is a function of z and t. The local properties inside the rarefaction wave at an instant in time can be found using Eq. (13) together with the following equations:

$$\frac{T}{T_4} = \left[1 - \frac{\gamma_4 - 1}{2}\left(\frac{u}{a_4}\right)\right]^2, \tag{22}$$

$$\frac{p}{p_4} = \left[1 - \frac{\gamma_4 - 1}{2}\left(\frac{u}{a_4}\right)\right]^{2\gamma_4/(\gamma_4 - 1)}, \tag{23}$$

$$\frac{p}{p_4} = \left[1 - \frac{\gamma_4 - 1}{2}\left(\frac{u}{a_4}\right)\right]^{2/(\gamma_4 - 1)}. \tag{24}$$

RESULTS AND DISCUSSION

Calculations were carried out to study the laser ablation process at different laser intensities, back temperatures, back pressures, and ambient gas species. The calculations simulate a graphite target subject to the heating of a KrF excimer laser, which has a laser pulse of 10 ns duration and laser radius of 1 mm. The material properties of graphite used by Zhang, Han, and Dulikravich[12] were adopted for the current study and are listed in Table I. Plots at the end of the 10 ns laser pulse are presented in Figs. 3–7.

Figure 3 shows the comparison between the analytical model and a numerical model developed earlier.[12] The laser energy is 0.2 J/pulse (corresponds to a laser intensity of 6.4×10^8 W/cm^2) and the ambient gas is argon at a temperature of 300 K and pressure of 1 kPa. A shock wave can be clearly seen in the figure, which propagates at a supersonic speed into the quiescent air (region 1) and sets up the gas behind it in motion in the direction of the shock wave. In the meantime, a rarefaction wave generated from the quiescent air propagates in the opposite direction into the high-pressure vapor. The shock wave and the rarefaction wave interact in such a manner as to establish a common pressure and velocity for the gas downstream of these waves (regions 2 and 3). The contact surface can be clearly seen between regions 2 and 3 in Fig. 3. The pressure and velocity are continuous across the contact surface, while the temperature, density, and entropy are discontinuous. While flow across the rarefaction wave is isentropic, flow across the shock wave is highly irreversible and follows the Rankine-Hugoniot relation. The analytical model agrees well with the numerical model in the rarefaction wave region. While the theoretical shock wave front shows very steep change in pressure, density, velocity, and temperature, the shock wave is smeared in the numerical simulation. This is due to the numerical dissipation inherent in the numerical model.

As expected, Fig. 3 shows that the temperature of the vapor decreases as the vapor expands. The temperature rises sharply behind the shock wave front due to the shock wave heating. The pressure and density of the vapor are the highest at the solid-vapor interface. They decrease monotonically as the vapor moves to the right. The local velocity increases as the vapor expands and reaches its peak at the start of region 3. The velocity remains constant at the peak value until it decreases sharply to 0 beyond the shock wave front.

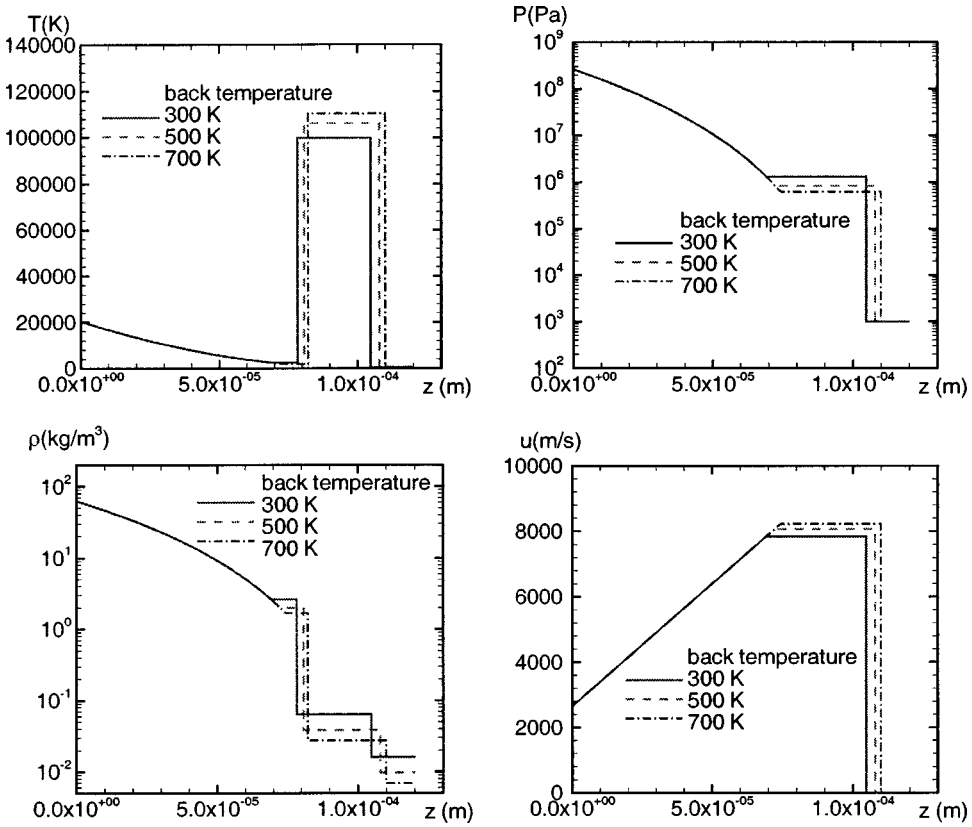

FIG. 5. Profiles of temperature, pressure, density, and velocity of the laser induced plume for different back temperatures.

The parameters used in Fig. 3 are also used in Figs. 4–7, unless otherwise indicated. Figure 4 shows the profiles of the temperature T, pressure p, density ρ, and velocity u of the laser induced plume for three different laser intensity levels. The laser energy levels are 0.2, 0.1, and 0.04 J/pulse, respectively. Since the surface temperature of the laser target increases with increasing laser intensity, the temperature and pressure of the vapor leaving the solid surface increase with increasing laser intensity as well. An increase of pressure and temperature in the vapor leaving the solid surface results in an increase of the pressure and temperature ratios in Eq. (14), which leads to greater shock wave strength p_2/p_1. Ratios of temperature, pressure, density, and velocity across the shock wave are proportional to the shock wave strength. Since the ambient conditions are constant for all three cases, Fig. 4 shows that the temperature, pressure, density, and velocity to the left of the shock wave front are the highest for laser energy of 0.2 J/pulse. The maximum temperature achieved by the laser induced plume ranges from 60 000 to 100 000 K for the three laser intensity levels studied. The trend agrees with experimental results available in the literature[26,27] that the maximum value of the kinetic-energy distribution of the emitted particles increases almost linearly over a range of low to moderate laser fluence. Quantitative comparison with the experimental studies cannot be made, since the ambient conditions in the experiments were not given. Previous studies, as well as the current paper, show that the laser ablation process is strongly influenced by the ambient conditions (see discussion later). The pressure, density, and local velocity increase with increasing laser intensity. The shock wave Mach number is also proportional to the shock wave strength. Figure 4 shows that the expansion velocity of the shock wave is the highest for laser energy of 0.2 J/pulse.

Figure 5 shows the profiles of the temperature, pressure, density, and velocity of the laser induced plume for three different back temperature levels (300, 500, and 700 K). Since the laser intensities for all three cases are identical, all thermodynamic and flow properties of the vapor leaving the solid surface are the same for all three cases. They remain the same through the start of region 3. As the back temperature increases, a_1/a_4 increases, which leads to a weaker shock wave strength p_2/p_1 [Eq. (14)]. Weaker shock wave strength leads to lower ratios of temperature, density, and velocity across the shock wave. While the ratios across the shock wave decrease with the decreased shock strength, the temperature of the laser induced plume increases due to the increased back temperature, as shown in Fig. 5. The maximum temperature achieved by the laser induced plume ranges from 100 000 to 110 000 K for the three back temperature levels studied. Since higher temperature leads to stronger plasma-laser beam interaction, these results can explain the experimental results reported by Braun, Zimmer, and Bigl, who observed that the ablation rate decreases with increasing ambient temperature. While the shock wave Mach number also decreases with the decrease of the shock wave strength, the background sound speed increases with the back temperature. Therefore, the shock wave velocity actually increase slightly with the back temperature, as can be seen in Fig. 5. In regions 2 and 3, the pressure and density of the laser induced plume decrease with the increase of the back temperature and the subsequent decrease of the shock wave strength. In the same regions, the local velocity of the

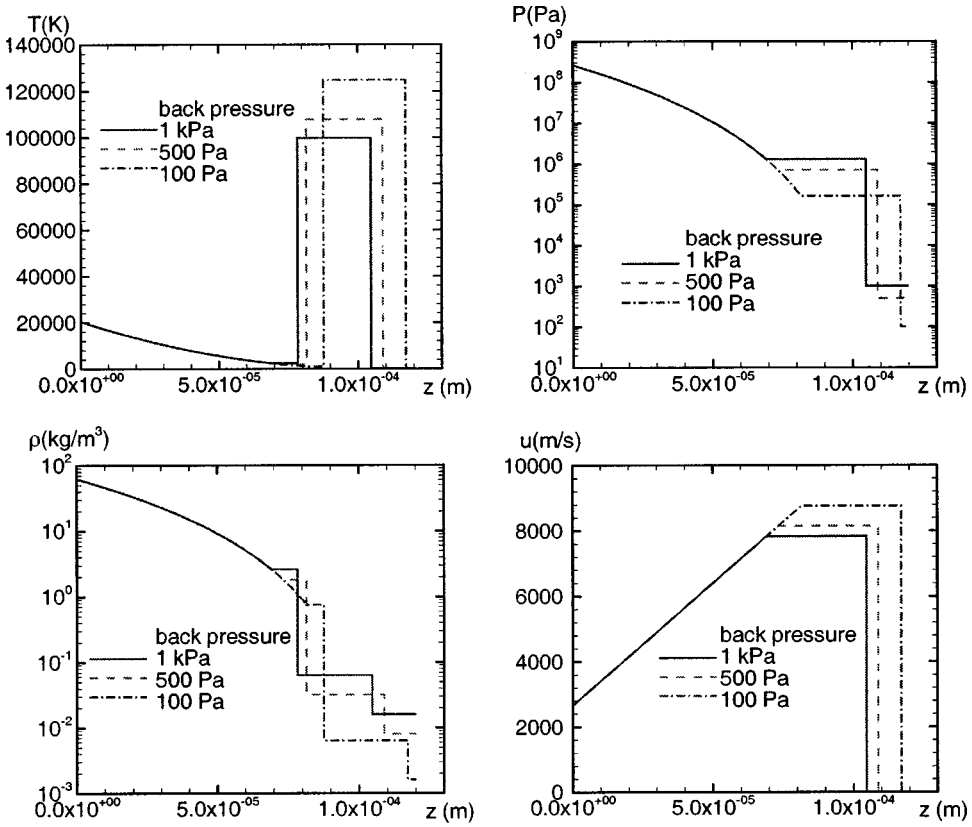

FIG. 6. Profiles of temperature, pressure, density, and velocity of the laser induced plume for different back pressures.

laser induced plume increases slightly with the increased back temperature.

Figure 6 shows the profiles of the temperature, pressure, density, and velocity of the laser induced plume for three different back pressure levels (1 kPa, 500 Pa, and 100 Pa). Again, since only the background conditions are changed, thermodynamic and flow properties of the vapor leaving the solid surface are the same and remain the same through the

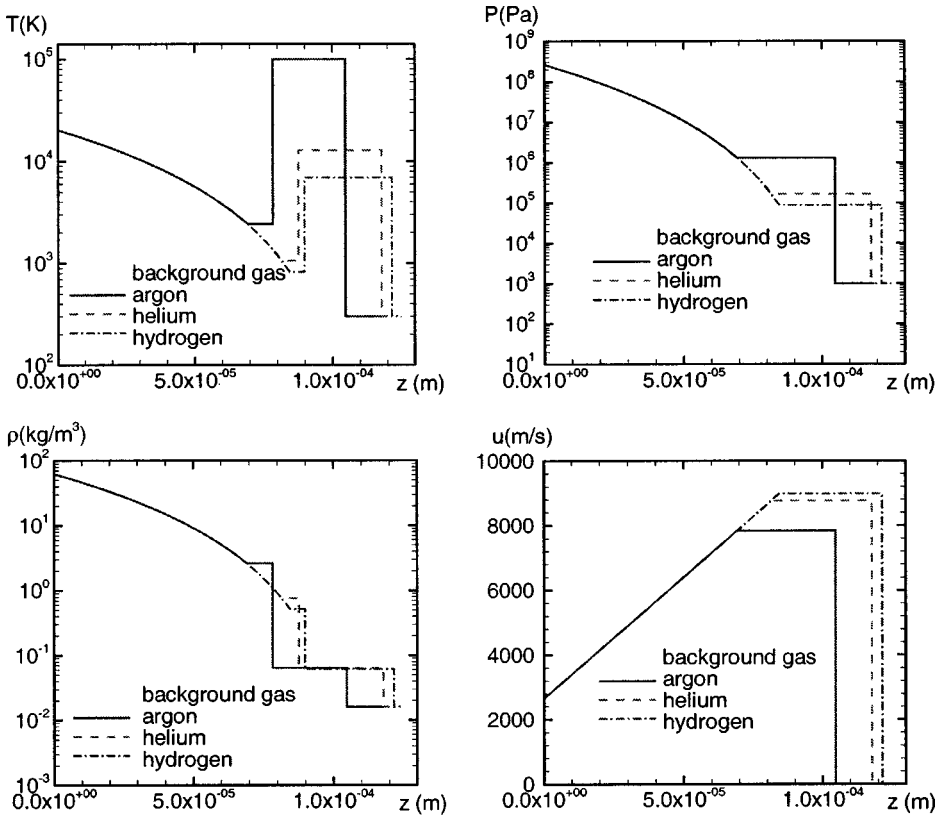

FIG. 7. Profiles of temperature, pressure, density, and velocity of the laser induced plume for different ambient gases.

start of region 3. The decrease of the back pressure results in greater p_4/p_1, leading to a stronger shock wave strength p_2/p_1, which further leads to greater ratios of temperature, density, and velocity across the shock wave. Figure 6 shows that the temperature and local velocity of the laser induced plume increase with the decrease of the back pressure. The maximum temperature achieved by the laser induced plume ranges from 100 000 K to slightly over 120 000 K for the three back pressure levels studied. The effects of ambient pressure on the temperature of the laser induced plume explain the experimental phenomena observed by Harilal,[22] who reported that the ambient pressure and laser intensity have opposite effects on the expansion process of the laser induced plume. While the ratios of the pressure and density increase with the decrease of back pressure, the pressure and density decrease due to the lower back pressure and density. The shock wave Mach number also increases with the increase in the shock wave strength. Since the background sound speed remains constant, the shock wave velocity increases with the decrease of the back pressure, as can be seen on Fig. 6.

Figure 7 shows the profiles of the temperature, pressure, density, and velocity of the laser induced plume for three different ambient gases (argon, helium, and hydrogen). The vapor leaving the solid surface has the same temperature, pressure, and velocity. Equation (14) shows that for a given pressure ratio p_4/p_1, the shock wave strength is made weak as a_1/a_4 is made greater. Therefore, ambient gases with low molecular weight lead to weak shock wave strength. Weaker shock wave strength implies lower temperature of the laser induced plume. Figure 7 shows that the temperature of the laser induced plume with hydrogen as the ambient gas is an order of magnitude lower than that with argon as the ambient gas. Higher temperature of the laser induced plume leads to stronger plasma-laser beam interaction. These results agree with previous experimental findings,[20,21] which show that the ablation rate decreases with increasing molecular weight. The weaker shock wave strength leads to smaller ratios of pressure and density across the shock wave front. While the shock wave Mach number is the smallest for hydrogen ambient gas, the shock wave velocity is the highest due to the large sound speed of hydrogen ambient gas.

CONCLUSIONS

A theoretical model of the laser ablation process is presented in this paper. The conduction inside the solid and the flow through the discontinuity layer are solved numerically, whereas the expansion of the high-temperature vapor is solved analytically. Calculations were carried out to simulate the laser ablation process from a graphite target subject to KrF excimer laser irradiation. The effects of the laser intensity, back temperature, back pressure, and ambient gas species on the laser induced plume have been studied using the theoretical model.

The simulations show that the laser ablation process is strongly influenced by the back temperature, back pressure, and ambient gas species, in addition to the laser intensity. The increase of the laser intensity leads to the increase of the temperature, pressure, density, and the shock wave velocity of the laser induced plume. This finding is in agreement with earlier experimental and numerical studies. The temperature and the shock wave velocity of the laser induced plume increase with the increase of the back temperature, while the pressure and density of the laser induced plume decrease with the increase of the back temperature. The temperature and the shock wave velocity of the laser induced plume increase with the decrease of the back pressure, while the pressure and density decrease with the decrease of the back pressure. Finally, the temperature, pressure, and density of the laser induced plume decrease with the decrease of the molecular weight of the ambient gas, while the shock wave velocity increases with the decrease of the molecular weight of the ambient gas.

ACKNOWLEDGMENT

The financial support of the National Aeronautics and Space Administration through Grant No. NGT5-40104 supplement 003 is gratefully acknowledged.

[1] J. F. Ready, *Effects of High-Power Laser Radiation* (Academic Press, New York, 1971).
[2] S. Anisimov, Sov. Phys. JETP **27**, 182 (1968).
[3] N. Bloembergen, Mater. Res. Soc. Symp. Proc. **51**, 3 (1985).
[4] C. J. Knight, AIAA J. **17**, 519 (1979).
[5] N. Krokhin, in *Physics of High Energy Density*, edited by P. Caldirola, and H. Knoepfel (Academic Press, New York, 1971).
[6] V. N. Tokarev, J. G. Lunney, W. Marine, and M. Sentis, J. Appl. Phys. **78**, 1241 (1995).
[7] F. Dahmani, Phys. Fluids B **4**, 1585 (1992).
[8] F. Dahmani, J. Appl. Phys. **74**, 622 (1993).
[9] A. Kar and J. Mazumder, Phys. Rev. E **49**, 410 (1994).
[10] J. R. Ho, C. P. Grigoropoulos, and J. A. C. Humphrey, J. Appl. Phys. **78**, 4696 (1995).
[11] J. R. Ho, C. P. Grigoropoulos, and J. A. C. Humphrey, J. Appl. Phys. **79**, 7205 (1996).
[12] Z. Zhang, Z. Han, and G. S. Dulikravich, J. Appl. Phys. **90**, 5889 (2001).
[13] S. S. Mao, X. Mao, R. Grief, and R. E. Russo, Appl. Phys. Lett. **76**, 3370 (2000).
[14] A. V. Bulgakov and N. M. Bulgakova, J. Phys. D **28**, 1710 (1995).
[15] R. Kelly and B. Braren, Appl. Phys. B: Photophys. Laser Chem. **53**, 160 (1991).
[16] R. Kelly, A. Miotello, B. Braren, and C. E. Otis, Appl. Phys. Lett. **60**, 2980 (1992).
[17] P. E. Dyer, P. H. Key, D. Sands, H. V. Snelling, and F. X. Wagner, Appl. Surf. Sci. **86**, 18 (1995).
[18] S. H. Jeong, R. Greif, and R. E. Russo, Appl. Surf. Sci. **127–129**, 177 (1998).

[19] D. B. Geohegan, in *Pulsed Laser Deposition of Thin Films*, edited by D. B. Chrisey and G. K. Hubler (Wiley Interscience, New York, 1994).
[20] X. L. Mao, W. T. Chan, and R. E. Russo, Mater. Res. Soc. Symp. Proc. **285**, 187 (1993).
[21] M. Mendes and R. Vilar, Appl. Surf. Sci. **206**, 196 (2003).
[22] S. S. Harilal, Appl. Surf. Sci. **172**, 103 (2001).
[23] A. Braun, K. Zimmer, and F. Bigl, Appl. Surf. Sci. **154–155**, 73 (2000).
[24] Z. Zhang, Numer. Heat Transfer, Part A **40**, 497 (2001).
[25] J. D. Anderson, *Modern Compressible Flow with Historical Perspective* (McGraw-Hill, New York, 1982).
[26] F. Muller and K. Mann, Diamond Relat. Mater. **2**, 233 (1993).
[27] K. J. Koivusaari, J. Levoska, and S. Lepavuori, J. Appl. Phys. **85**, 2915 (1999).